Tokyo, Japan
National Graduate Institute for Policy Studies

Tsukuba, Japan
Building Research Institute

PRELIMINARY ANALYSIS FOR EVALUATION OF LOCAL SITE EFFECTS IN LIMA CITY, PERU FROM STRONG GROUND MOTION DATA BY THE SPECTRAL INVERSION METHOD

A Master Paper
Submitted in Partial Fulfillment of the Requirement
For the Degree of Master in Disaster Management

By QUISPE GAMERO Mileyvi Selene（MEE09185）

Disaster Management Policy Program （2009-2010）

（ Seismology ）

September 2010

Abstract

Local site, propagation path and source effects in observed strong motion records are separated by the spectral inversion method proposed by Iwata and Irikura (1986, 1988) to examine the relation between local subsurface conditions and the local site amplifications in the frequency range from 0.5 to 10 Hz. S-wave portions of accelerograms in horizontal components observed at 5 stations for 11 events along the Pacific coast of Lima city, Peru are analyzed. These events are superficial and intermediate earthquakes with local magnitudes from 4.0 to 5.7 and with hypocentral distances from 40 to 180 km. In the spectral inversion, it is assumed that the site amplification factor at a reference station CLDCIP is the same as that of the theoretical transfer function of S-waves to the soil model whose bottom layer has an S-wave velocity of around 780 m/s. The factors of site amplification $G_j(f)$ obtained in the present study are compared with the results obtained by Cabrejos (2009) for stations CSM, CAL, MOL and CDLCIP employing the standard spectral ratio (SSR) method, which support our results especially at frequencies below 5 Hz. Q_S-value obtained shows frequency dependency of the form $Q_S(f)=80.4f^{0.63}$. In addition, the influence of non-linearity on the site response is evaluated during the Pisco earthquake which it is concluded that nonlinear response of the soils was not detected at acceleration levels below 115.2 gal (the maximum peak ground acceleration recorded in Lima city) during this strong ground motion. The study also proposed relationships between the amplifications with average S-wave velocity in top 30 meters of the S-wave profiles for some stations at each frequency.

Keywords: Spectral Inversion Method, Lima city, Site Amplification, Q_S-value, Standard Spectral Ratio, Pisco earthquake

---

The author works for Japan Peru Center for Earthquake Engineering and Disaster Mitigation (CISMID), Lima city, Peru

Table of Contents

1. INTRODUCTION

Lima city, the capital and most densely-populated city of Peru, has been continuously affected by several earthquakes that have caused slight, considerable and severe damages. This city is prone to this kind of natural disaster due to the subduction of the Nazca plate underbeneath the South American plate. In the last 60 years, according to the earthquake catalog compiled by the Geophysical Institute of Peru (IGP), the city of Lima has been subjected to earthquakes with the biggest Mw of 8.1 (e.g., October 17, 1966 (Mw=8.1), May 31, 1970 (Mw=7.9), November 29, 1971 (Mw=5.9), January 5, 1974 (Mw=6.5), and October 3, 1974 (Mw=8.1)). According to the studies (Lee et al. (1968); Lomnitz and Cabré (1968)) most of these events have caused unusually low level of damages in the city itself compared with other places of the world subjected to similar earthquakes. The explanation of this is that a big portion of Lima city is underlain by a dense to very dense, gravelly fluvial, which is locally named as “Lima Conglomerate” or “Cascajo” (Repetto et al. 1980).

It is during the earthquake of October 3, 1974 (Mw=8.1) with focal depth about 13 km that a few areas outside of Lima center were severely damaged, such as La Campiña (Chorrillos), La Molina and Callao – La Punta (Repetto et al. 1980). According to Espinoza et al. (1977), the maximum Modified Mercalli intensity observed in these areas was of IX. Works described by Husid (1977), Espinoza et al. (1977), Repetto et al. (1980) and Stephenson et al. (2009) refer that these areas were affected by the influence of local subsurface conditions. For example, in La Molina district it was possible to observe collapse of reinforced concrete structures during the October 3, 1974, earthquake.

Nowadays many numerical techniques for estimating local site effects have been developed, including empirical methods, which have been developed based on inversion technique using observed seismic-wave records without detailed information on the subsurface structure (e.g., Andrews 1982; Iwata and Irikura 1988; Phillips and Aki 1986). The empirical method applied in this study is the spectral inversion method proposed by Iwata and Irikura (1986). This method simultaneously separates the source, propagation path, and local site effects from observed strong motion records for the purpose of empirical evaluation of the local site effects in different local subsurface conditions. This approach utilizes the direct S-waves.

The present study uses the strong motion records observed along the Pacific coast of Lima city, Peru, in which the seismic events were recorded by 5 stations in 4 years (2005-2008). The relation between local subsurface conditions and the local site effect in some areas of Lima city are discussed based on the results obtained from the spectral inversion method.

2. DATA & DATA PROCESSING

2.1 Data

The analyzed data are the S-wave portions of 30 accelerograms from 11 events observed at 5 strong ground motion recording stations. Out of the five stations used in this study, four stations belong to the CISMID Accelerometer Network: CSM, CAL, MOL and CDLCIP stations, and one station, LMO station belongs to the Geophysical Institute of Peru (IGP). Figure 1 and Figure 2 show the locations of observation stations and epicenters determined by the CISMID Accelerometer Network and the IGP, respectively. Table 1 shows detailed information about the location of accelerographic stations and the number of available recordings per station; and Table 2 is observed details of the strong ground motion data, such as date-time, location, local magnitude (ML), focal depth, and seismic stations that detected the event with its respective hypocentral distances.

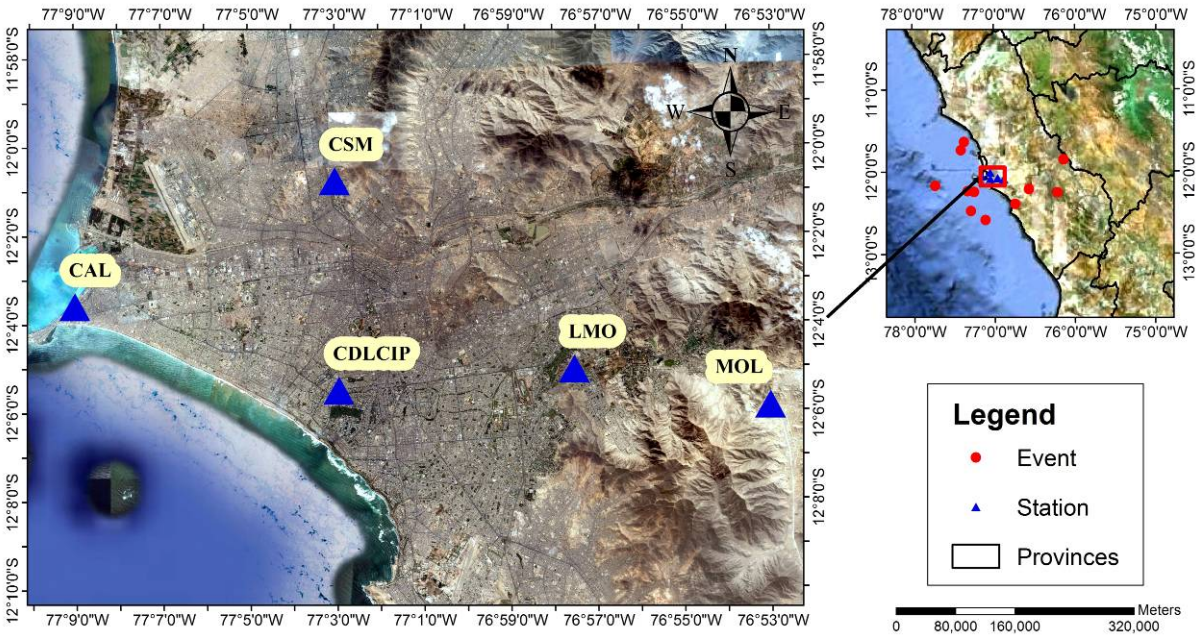

Figure 1. Location of observation stations. CSM, CAL, MOL and CDLCIP stations belong to the CISMID Accelerometer Network, and LMO station belongs to the Geophysical Institute of Peru (IGP).

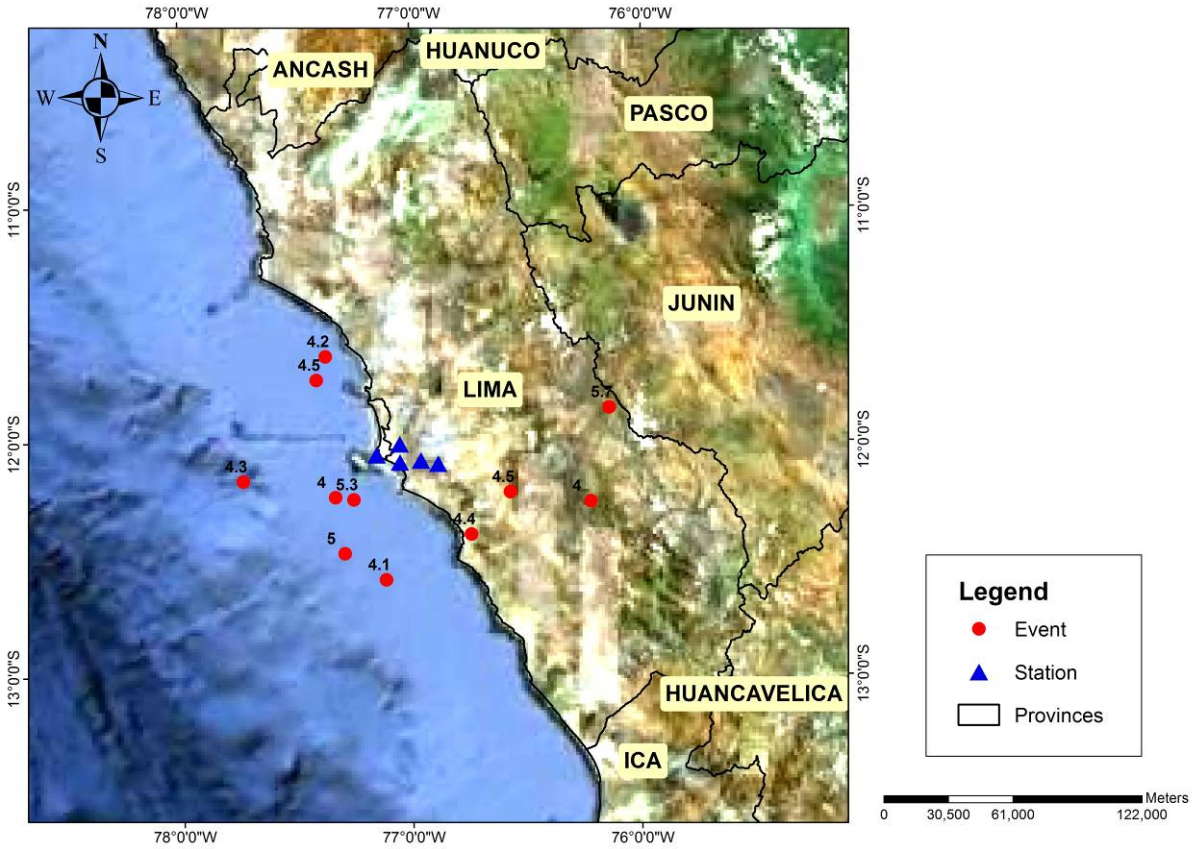

Figure 2. Location of epicenters of events used in this study determined by the Geophysical Institute of Peru (IGP).

Table 1. List of coordinates and number of available records per site.

Station Province	Station District	Code Station	Longitude (deg)	Latitude (deg)	Number of data
Lima	Independencia	CSM	-77.05	-12.01	10
Lima	Callao	CAL	-77.15	-12.06	6
Lima	La Molina	MOL	-76.89	-12.10	8
Lima	San Isidro	CDLCIP	-77.05	-12.09	2
Lima	La Molina	LMO	-76.95	-12.08	4

Table 2. Parameters and recorded sites for the earthquake used in this study.

No	Yr	MD	HM	Longitude (deg)	Latitude (deg)	Local Magnitude (ML)	Depth (km)	Station	Hypocentral Distance (km)
1	2005	0302	0848	-76.14	-11.86	5.7	124	CSM, CAL, MOL	159.8, 167.3, 151.0
2	2005	0719	0845	-77.11	-12.59	4.1	48	CSM, MOL	80.4, 76.6
3	2005	0725	0151	-77.33	-12.24	4.0	42	CSM, MOL	57.7, 65.7
4	2005	1014	0001	-76.74	-12.4	4.4	74	CSM, CAL, MOL	92.0, 94.3, 82.9
5	2005	1110	1138	-76.22	-12.26	4.0	71	CSM, CAL, MOL	118.2, 125.6, 103.4
6	2005	1227	1202	-76.57	-12.22	4.5	99	CSM, MOL	114.4, 105.9
7	2006	0525	2057	-77.41	-11.74	4.5	38	CSM, MOL, LMO	62.5, 79.1, 73.4
8	2006	1211	1653	-77.37	-11.64	4.2	54	CAL, MOL, LMO	75.2, 90.9, 86.0
9	2008	0329	0140	-77.73	-12.17	4.3	48	CSM, CAL, CIP	90.0, 80.3, 88.8
10	2008	0329	0751	-77.25	-12.25	5.3	51	CSM, CAL, CIP, LMO	61.4, 56.3, 58.3, 63.6
11	2008	0607	0806	-77.29	-12.48	5.0	67	CSM, CAL, LMO	88.6, 83.0, 88.6

In Figure 3, the seismic events are superficial and intermediate earthquakes (depth < 140 km) from 40 to 180 km in hypocentral distance. The observed peak ground accelerations (PGA) range from 5.5 to 109.0 gal (Figure 4), so the coverage over PGAs implies that there is very small possibility of non-linear effect. Besides, the ML is ranging from 4.0 to 5.7, therefore the coverage over ML of the analyzed data implies a simple source process and source size small enough in comparison with the hypocentral distances. So, the assumption of the point source and omega square source spectra can be used.

These seismic events are chosen for this analysis because they are located in a subducting slab and also have appropriate hypocentral distances in consideration of the propagation paths of direct S-waves from source to station that do not cause instability in the solution.

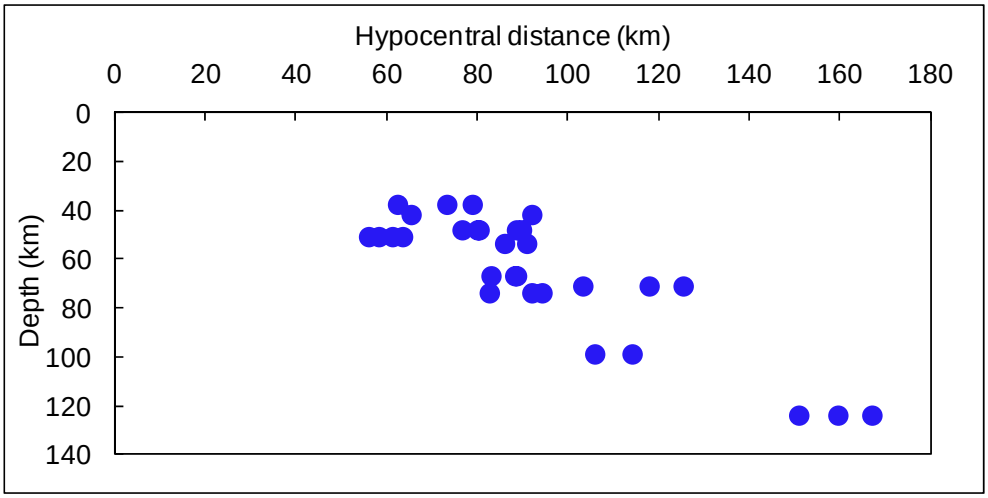

Figure 3. Distribution of distance and depth.

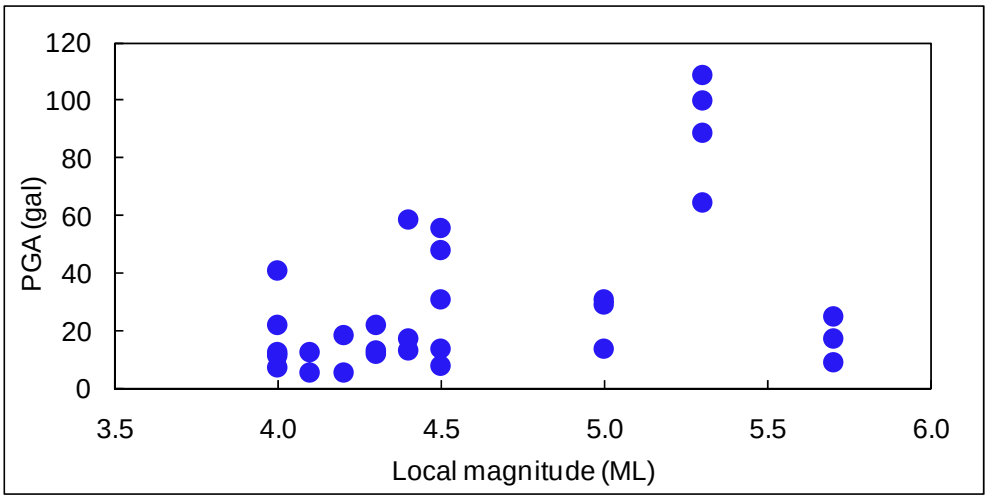

Figure 4. Distribution of magnitude and PGA

The main objective of the present study is to analyze the relation between the local subsurface conditions and the local site amplifications, so it is necessary to know the geology where the stations are located. If you see Figure 5, most part of Lima city is underlain by a dense to very dense, gravelly fluvial material deposited by the Rimac River, locally named as “Lima Conglomerate” or “Cascajo”. The Lima Conglomerate is the local name for a sandy, bouldery gravel, poorly graded, but usually very dense, with rounded cobbles and boulders up to 50 cm in diameter (Repetto et al. 1980). According to Le Roux et al. (2000), the Lima Conglomerate has a thickness of at least 86 m.

Also in Figure 5 is shown the location of the stations used for this study on the geological map of Lima city (Martinez et al. 1975), and Table 3 exhibits the geological period at each station and the average shear-wave velocity to 30 meters (Vs30) for some stations.

According to the geological map of Lima city (Martinez et al. 1975), CSM and CDLCIP stations are located on alluvial soil deposits belonging to the Quaternary Holocene (Figure 5).

One-dimensional shear-wave velocity profile for these stations was obtained using the Multichannel Analysis of Surface Wave (MASW), and the Vs_{30} is 533.23 m/s and 565.82 m/s, respectively (R. Piedra, personal communication).

CAL station is located on Quaternary alluvial deposits of the Rimac River (Martinez et al. 1975). The shallow coverage of deposits consists of soft clays (Bernal and Tavera 2007). There is no information regarding the S-wave velocity profile obtained through geophysical methods, but Bernal and Tavera (2007) estimated the S-wave velocity profile by an inversion of spectral ratios (H/V and standard techniques). Vs_{30} parameter is 104.79 m/s.

MOL station is also located on shallow soil overlying the denser Lima Conglomerate, and MLO station is located on cretaceous intrusive rock (Figure 5). As in the previous case, Bernal and Tavera (2007) estimated the S-wave velocity profile for MOL station but up to a depth of about 20 meters. In LMO station, up to now, there is no available information regarding the S-wave velocity profile.

The S-wave velocity profiles for the stations mentioned above are shown in Appendix-A.

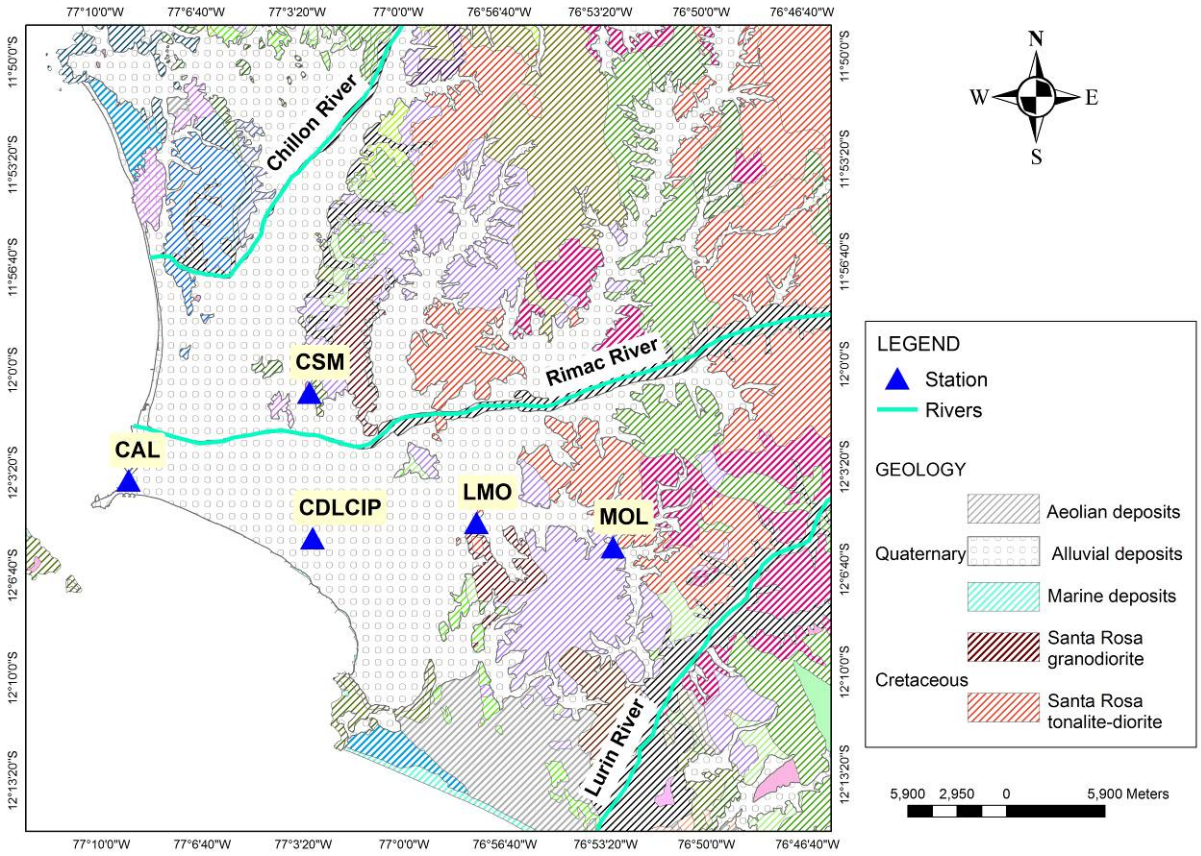

Figure 5. Locations of stations on the geological map of Lima city (Martinez et al. 1975).

Table 3. Surface geology of the stations.

Code Station	Geological period	Geology	Vs_{30} (m/s)
CSM	Quaternary	Alluvial	533.23
CAL	Quaternary	Alluvial	104.79
MOL	Quaternary	Alluvial	---
CDLCIP	Quaternary	Alluvial	565.82
LMO	Cretaceous	Santa Rosa Granodiorite	---

2.2 Data Processing

The spectral inversion method utilizes the direct S-waves, so the S-wave portions of two horizontal components (NS and EW) of seismic ground motions are analyzed after the instrumental correction (Takemura et al. 1991). To recognize the onset time of S-wave, particle motion plots for two components of motion, EW component on the horizontal axis and NS component on the vertical axis (Figure 6), and Husid plots (Husid et al. 1969) where the horizontal axis is the time and vertical axis is the accumulated horizontal component square for each horizontal component (Figure 7) are realized.

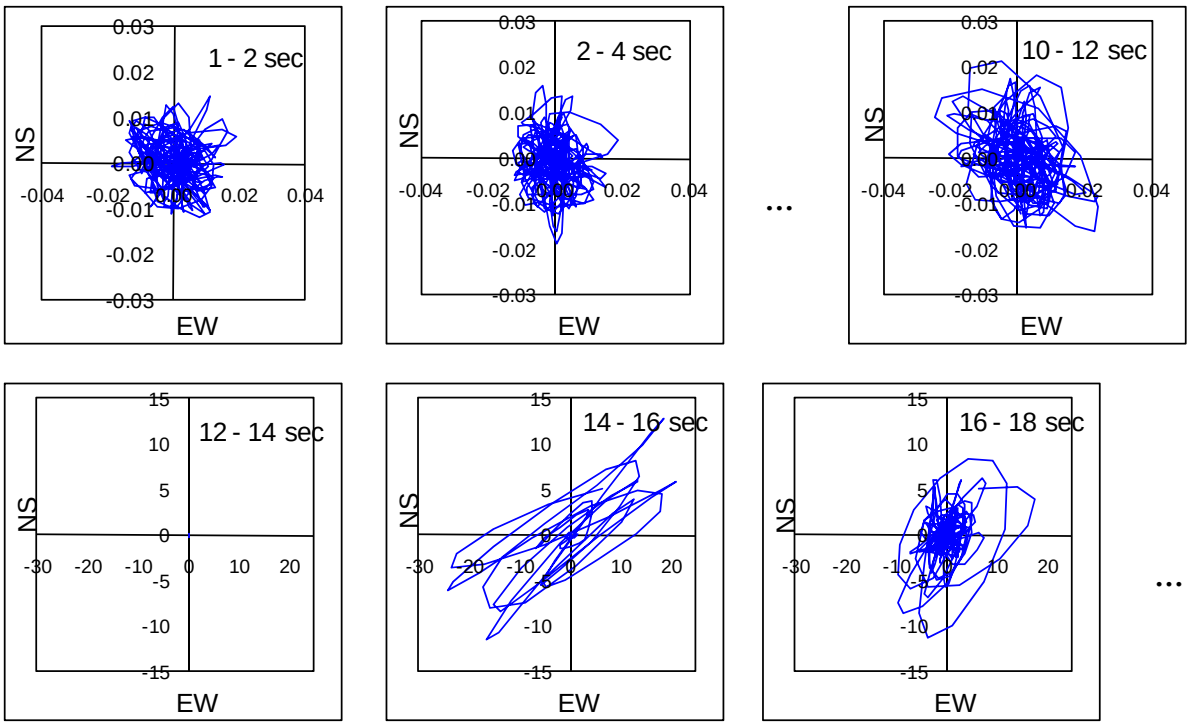

Figure 6. Particle motion plots for two components of motion.

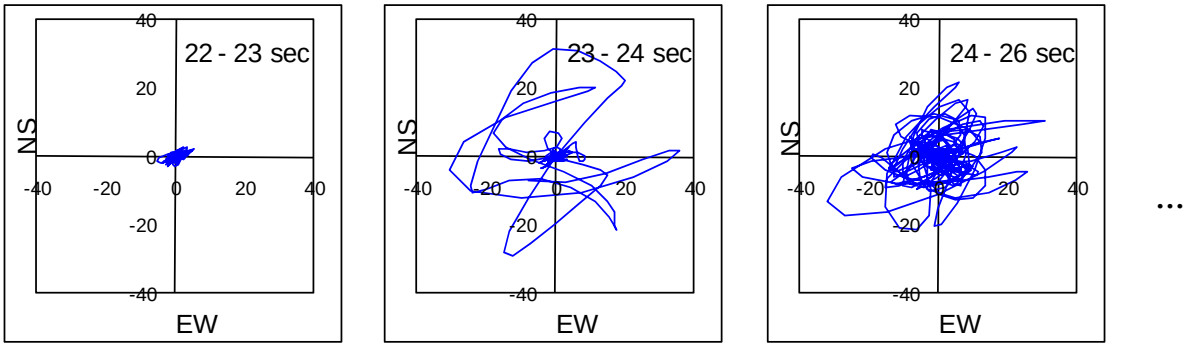

Figure 6. Particle motion plots for two components of motion.

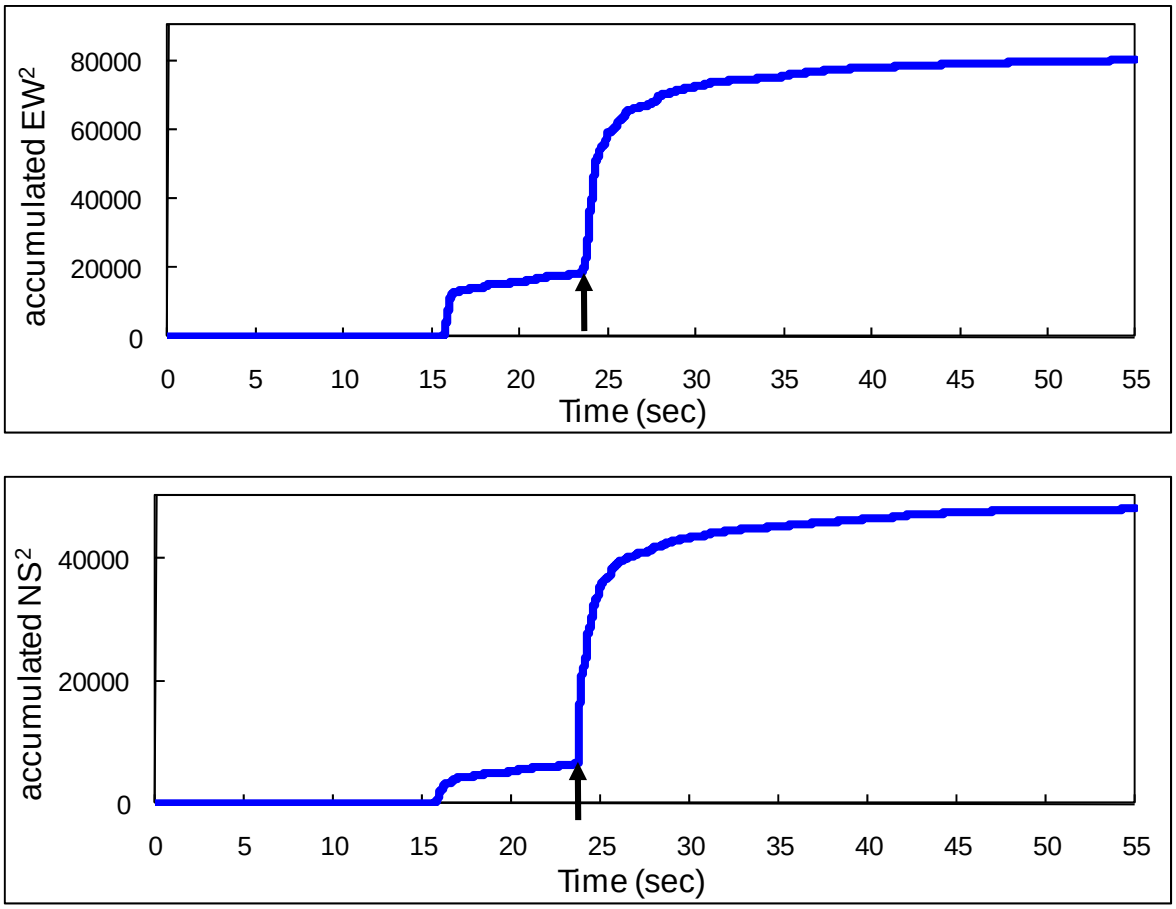

Figure 7. Husid plots to recognize the onset time of S-wave. The horizontal axis is the time and vertical axis is the accumulated horizontal component square for each horizontal component. Black arrows indicate the S-wave onset time.

From Figure 7, the onset time of S-wave can be determined clearly because of the quick change of accumulated energy represented by black arrows, at which a close-up of the exact position of the S-wave onset time was done to make sure.

After the onset time of S-wave has been determined, the S-wave portion of accelerograms (*to*) is extracted. The value of '*to*' depends on the earthquake magnitude. A cosine-type tapered data-window has been applied to S-wave portion to improve the problem of finite record length using the same criterion took by Takemura et al. (1990) (Figure 8). Fourier acceleration amplitude spectra (FAAS) of two horizontal components are computed and summed vectorially. To be sure that '*to*' is taking the appropriate S-wave portion, at least three different '*to*' has been taken, and to repeat the previous steps to compare the FAAS for different '*to*' in the frequency range from 0.5 to 10.0 Hz, and to finally to decide which '*to*' should be taken. For example for a seismic event of ML=4.0, the probable '*to*' would be 4, 5 and 6 sec.

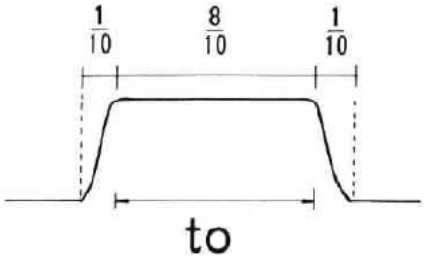

Figure 8. Data window adopted for analysis of accelerograms (Takemura et al. 1990).
'*to*' is the analyzed portions of the S-wave.

Table 4 shows the data length for the analysis (*to*), which is determined by considering the duration time of faulting estimated from the earthquake magnitude, as previously said.

Table 4. The S-wave portion of accelerograms (*to*) for each seismic event.

No.	Date	ML	*to* (sec)
1	2005/03/02	5.7	7.0
2	2005/07/19	4.1	5.0
3	2005/07/25	4.0	5.0
4	2005/10/14	4.4	5.0
5	2005/11/10	4.0	5.0
6	2005/12/27	4.5	5.0
7	2006/05/25	4.5	5.0
8	2006/12/11	4.2	5.0
9	2008/03/29	4.3	5.0
10	2008/03/29	5.3	8.0
11	2008/06/07	4.1	5.0

Before using the inversion scheme, the Fourier acceleration amplitude spectra were smoothed with seventeen-point moving average method (See Appendix-B).

3. METHOD of ANALYSIS

3.1 Spectral Inversion

One of the big advantages of the spectral inversion is separated source, propagation path, and local site effects from observed seismic waves to examine the relation between local site effects and surface geology (Takemura et al. 1991). In the present study, we adopt the inversion method by Iwata and Irikura (1986, 1988). They assume the quality factor of the wave propagation is independent from the path and only depends on frequency (i.e., Q=Q(f)). Then the observed S-wave Fourier amplitude spectrum is expressed by

$$O_{ij}(f) = S_i(f)G_j(f)R_{ij}^{-1}\exp\left(-\pi R_{ij} f \Big/ Q_s(f)Vs\right) \tag{1}$$

where, $O_{ij}(f)$, observed S-wave Fourier amplitude spectrum of i-th event at j-th station; $S_i(f)$, source amplitude spectrum of i-th event; $G_j(f)$, factor of site amplification at j-th station; R_{ij}, hypocentral distance between i-th event and j-th station; $Q_S(f)$, average Q_S-value along the wave propagation path; V_S, average S-wave velocity along the wave propagation path (=3.7 km/s) (Kato et al. 1992).

This equation assumes a point source solution for the S-waves in an infinite elastic medium and that source amplitude spectrum for $S_i(f)$ can be written as

$$S_i(f) = R_{\theta\phi}M(f)\Big/4\pi\rho v_S^3 \tag{2}$$

where, $M(f)$, is seismic moment density; $R_{\theta\phi}$, is the radiation pattern coefficient; ρ, is the density; v_S, is the S-waves velocity (Kanamori 1972).

To separate source, path, and site effects simultaneously from spectra of observed seismic waves as described hereafter, the first step is to take the logarithm of Eq. (1) to obtain simultaneous logarithmic equations in the form.

$$\log O_{ij}(f) = \log S_i(f) + \log G_j(f) - (\pi f / Q_S(f)V_S)R_{ij} \tag{3}$$

These equations have unknown parameters of I (source terms) + J (site amplification

terms) + 1 (Q_S – value), which can be determined by the least squares method from IxJ data for Oij(f) at each frequency. However, there is still one unconstrained degree of freedom. Therefore, a constraint condition is needed to determine the unknown parameters.

As a result of this need, Iwata and Irikura (1988) set up a constraint conditions that the site amplification factor must be 2 or over considering the free surface amplification. The constraint condition taking account is explained in the following subchapter.

3.2 Choice of Reference Site

The CDLCIP accelerometer station is used as a constraint condition for the inversion analysis, and the station is located on a shallow, dense to very dense coarse gravel (Figure 9 (a)). So, for inversion the factor of site amplification at a reference station CDLCIP is assumed to be the same as that of theoretical amplification of S-wave (Ozmen, 2009) (Figure 9 (b)). The factor of site amplification is constrained from 2 to about 5. This constraint condition represents the free surface amplification effect.

Figure 9 (a) shows the shear wave velocity profile (Vs) of this station, which was obtained by conventional Multi-Channel Analysis of Surface Waves method (MASW), and Figure 9 (b) shows the site amplification factor of $G_j(f)$. The parameters of structure at CDLCIP station are shown in Table 5 (R. Piedra, personal communication). The quality factor Q is assumed as "$Qs=Vs/10$" where Vs is the shear velocity in m/s.

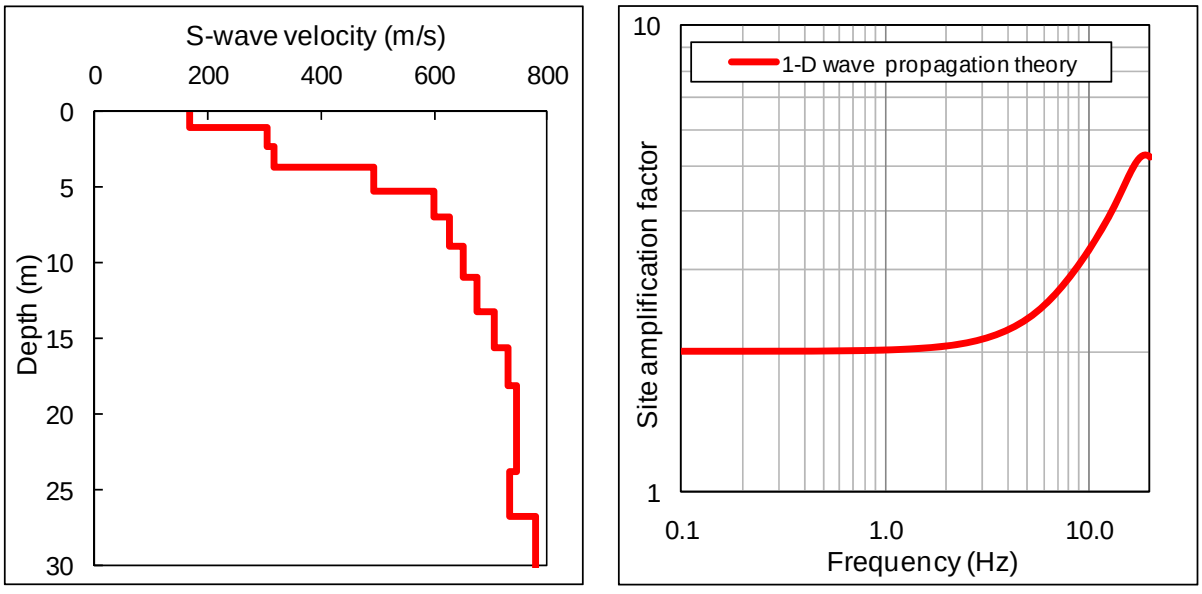

(a) (b)

Figure 9. (a) Subsurface shear-wave velocity at CDLCIP station (b) Result of transfer function of SH wave at this station.

Table 5. The parameter of structures at CDLCIP station (R. Piedra, personal communication).

Layer	S-wave velocity (m/s)	Density (g/cm^3)	Thickness (m)	Q-value
1	169	1.8	1.1	17
2	304	1.8	1.2	30
3	318	1.8	1.4	32
4	494	1.9	1.6	49
5	599	2.0	1.7	60
6	627	2.0	1.9	63
7	651	2.0	2.1	65
8	677	2.0	2.2	68
9	706	2.0	2.4	71
10	731	2.0	2.6	73
11	745	2.0	2.7	75
12	745	2.0	2.9	74
13	734	2.0	3.0	73
14	780	2.0	∞	78

4. RESULTS

4.1 Local Site Effect

Figure 10 shows the factor of site amplification factor obtained by the spectral inversion method $G_j(f)$ represented by the solid blue line. The S-wave velocity profile of some stations are known, so it is a good opportunity to calculate the theoretical transfer function and it is superposed in Figure 10 by the broken red line to compare both results.

For the CSM station, there is an apparent harmony between both results in high frequencies. The broad peaks and troughs of the theoretical transfer function correspond to the site amplification factor obtained by the inversion analysis.

For the CAL station, the narrow peaks and troughs of the theoretical transfer function can be identified in those of $G_j(f)$, but not all the peaks and troughs of the theoretical transfer functions are in agreement with the $G_j(f)$, since the data of the observed spectra used for the evaluation of $G_j(f)$ are smoothed in frequency domain (Kato et al. 1992).

For MOL station, the consistency between the theoretical transfer function and $G_j(f)$ can be seen only in high frequencies.

In the case of LMO station, information about the S-wave velocity profile is not available, so it is not possible to calculate the theoretical transfer function. However, as described previously, this station is located on intrusive rock, so the $G_j(f)$ is less compared with the other stations.

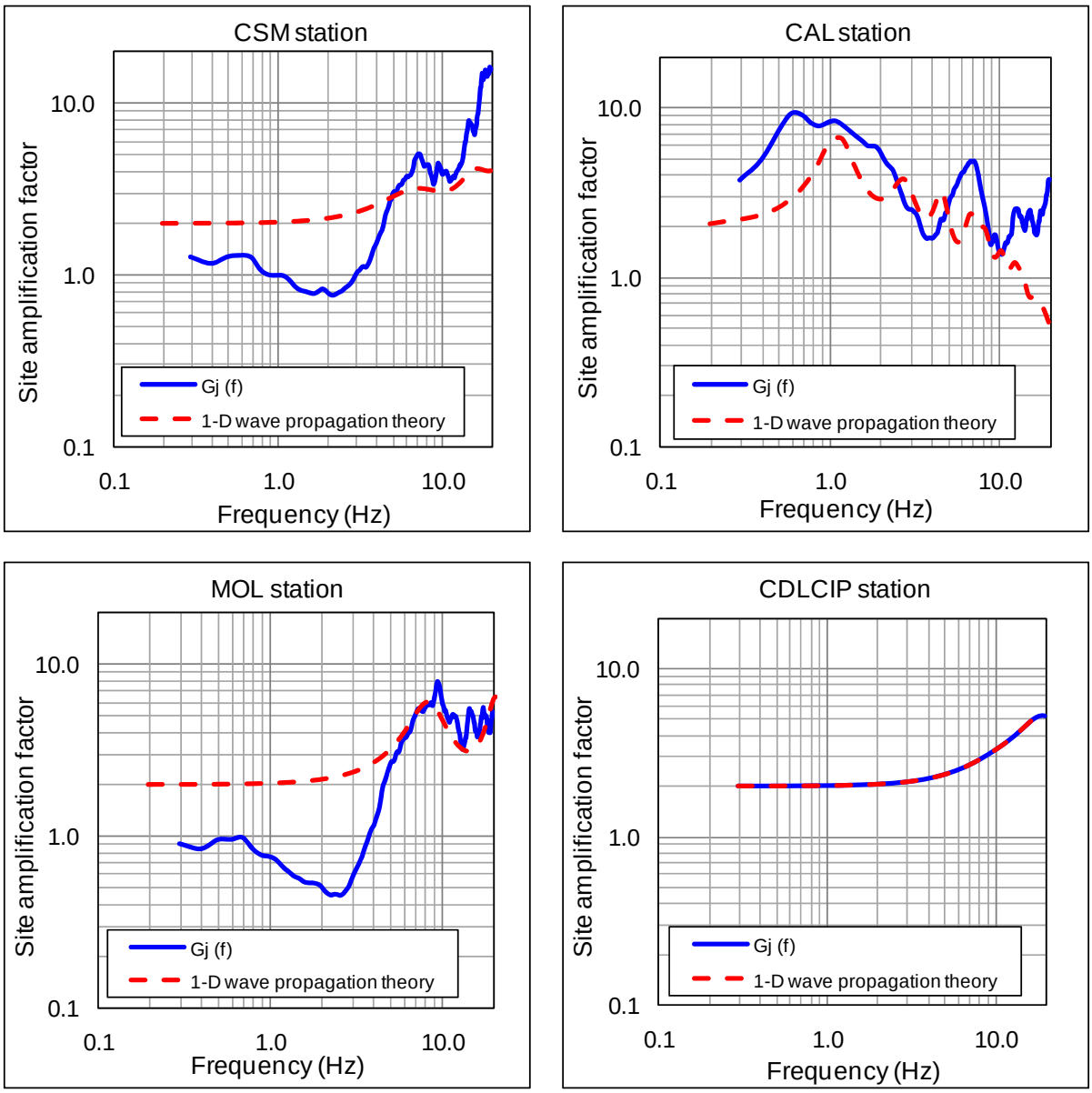

Figure 10. The character of site responses for each site.

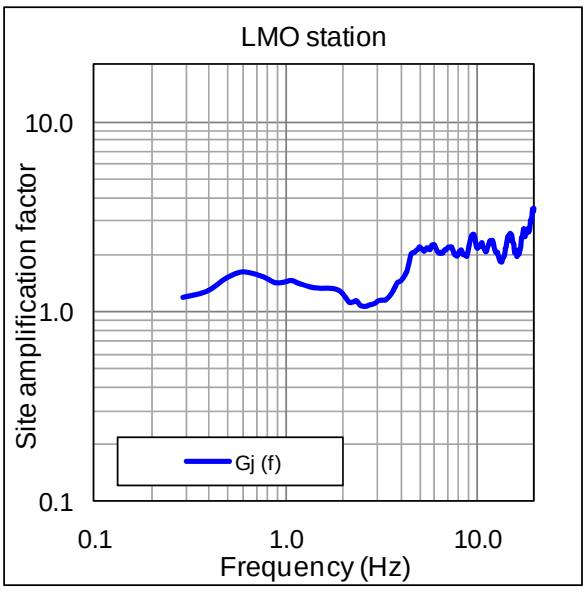

Figure 10. The character of site responses for each site.

4.2 Source Spectra and Q_S-values

The source acceleration amplitude spectra are obtained from the inversion technique. It is divided over ω^2 to obtain the source displacement spectra and to replace in the equation (2) to get the seismic moment density *M(f)*. The shear-wave velocity of 4.0 km/s, density of 3.0 g/cm^3, and the average point-source radiation coefficient of 0.6 are assumed. These coefficients were also assumed by Takemura et al. (1989) and Kato et al. (1991b). Figure 11 shows examples of the source spectra for events with ML from 4.0 to 5.7.

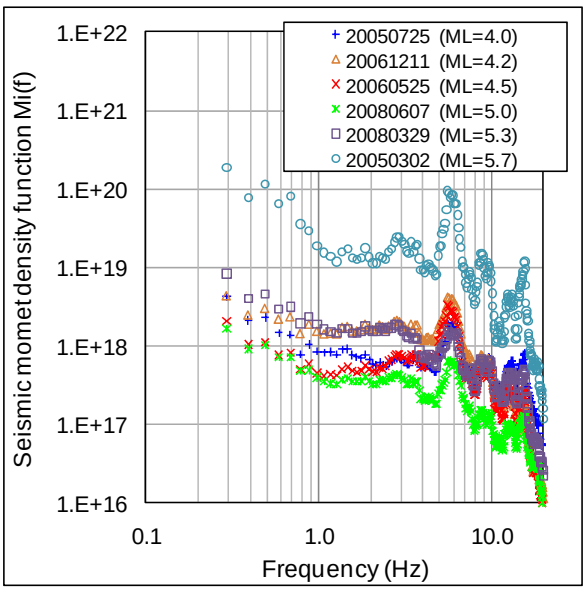

Figure 11. Examples of seismic moment density functions.

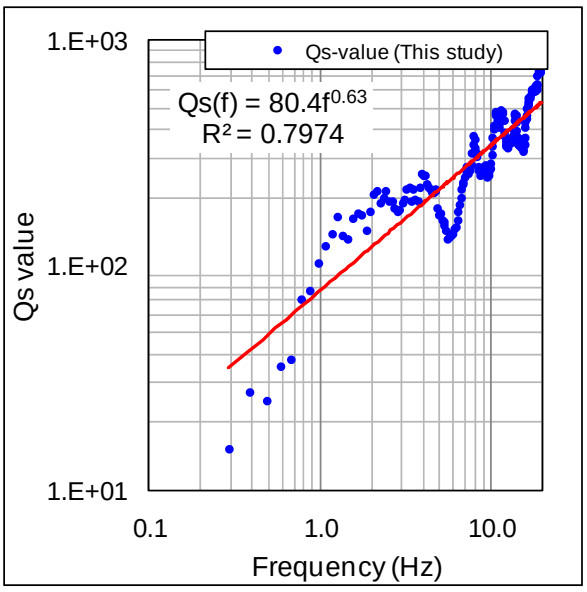

Figure 12. Q_S-values as a function of frequency.

Figure 12 shows the Q_S-values obtained by the inversion as a function of frequency and a formula of $Q_S(f)=80.4f^{0.63}$ which fits the results.

5. DISCUSSION

5.1 Site Amplification Factor and Standard Spectral Ratio

If the site amplification factor obtained by the spectral inversion method $G_j(f)$ (Figure 10) is examined, the first noticed result is that the $G_j(f)$, specially for CSM, MOL and LMO stations, is under the value 2 in frequencies lower than 5 Hz.

Cabrejos (2009) also estimated the amplifications of ground motions for the same stations evaluated in this study. For his study, he used the Standard Spectral Ratio (SSR). Since the spectral ratio is not necessary to know the S-wave velocity structure of the reference site, he used the LMO station, a station located on intrusive rock as reference site. Table 6 shows the data used by Cabrejos (2009). For example, the "green squares" represent the data used in his study, while the "blue squares" represent the data that he didn't use but was used in this study, and the "green and blue squares" represent the data that both two studies used.

Table 6. Data used by Cabrejos (2009).

					CISMID Accelerometer Network				Geophysical Institute of Peru (IGP)
	N°	Date	ML	Depth (km)	CSM	CAL	MOL	CDLCIP	LMO
2005	1	05/12/27	4.5	99					
2006	2	06/05/11	4.3	90					
	3	06/10/26	5.8	42					
	4	06/12/11	4.2	54					
2007	5	07/08/17	5.5	23					
	6	07/08/19	5.7	30					
2008	7	08/03/29	5.3	51					
	8	08/06/07	5.0	67					

Events used by Cabrejos (2009)
Events used in this study
Events used by both

The site amplification factor (SAF) obtained by the inversion method is compared with the spectral ratio obtained by Cabrejos (2009). It is important to know that the site amplification at all the sites is defined as the ratio of surface motion to the input motion from the bottom layer of the model for the reference site. On the other hand, the standard spectral ratio (SSR) is defined as the ratio of surface motion at each site to surface motion at the reference site. The definition of the SSR is different from the spectral inversion method, because the surface motion at the reference site is affected with the amplification of shallow soils due to weathering and the fractured nature of the rock in the near surface (Steidl et al. 1996). Besides, the propagation path effect is included in the SSR, but the SSR assumes that the path term will be cancel when the separation between stations is much less than their hypocentral distances from the source (like Cabrejos' study). On the contrary in the spectral inversion, the three effects are automatically separated.

Figure 13 displays a comparison between the site amplification factor $G_j(f)$ represented by the blue line and the SSR represented by the green line. Figure 13 explains that there is a good agreement between both results, especially in low frequencies, which support our results although different techniques for estimating site response have been applied and different reference sites have

been used, as previously mentioned. The peaks and troughs of the $G_j(f)$ can be identified in those of SSR, although the $G_j(f)$ values are smoothed in frequency domain.

It is noted from Figure 13, that $G_j(f)$ has large values at frequencies above 5 Hz compared with the SSR values, because the amplification at the reference site becomes large in this frequency range (Figure 9).

For CDLCIP station, the site amplification factor differs from the SSR, as previously mentioned, because both studies used different reference sites, CDLCIP station located on gravel deposits for this study and LMO station located on rock for Cabrejos' study.

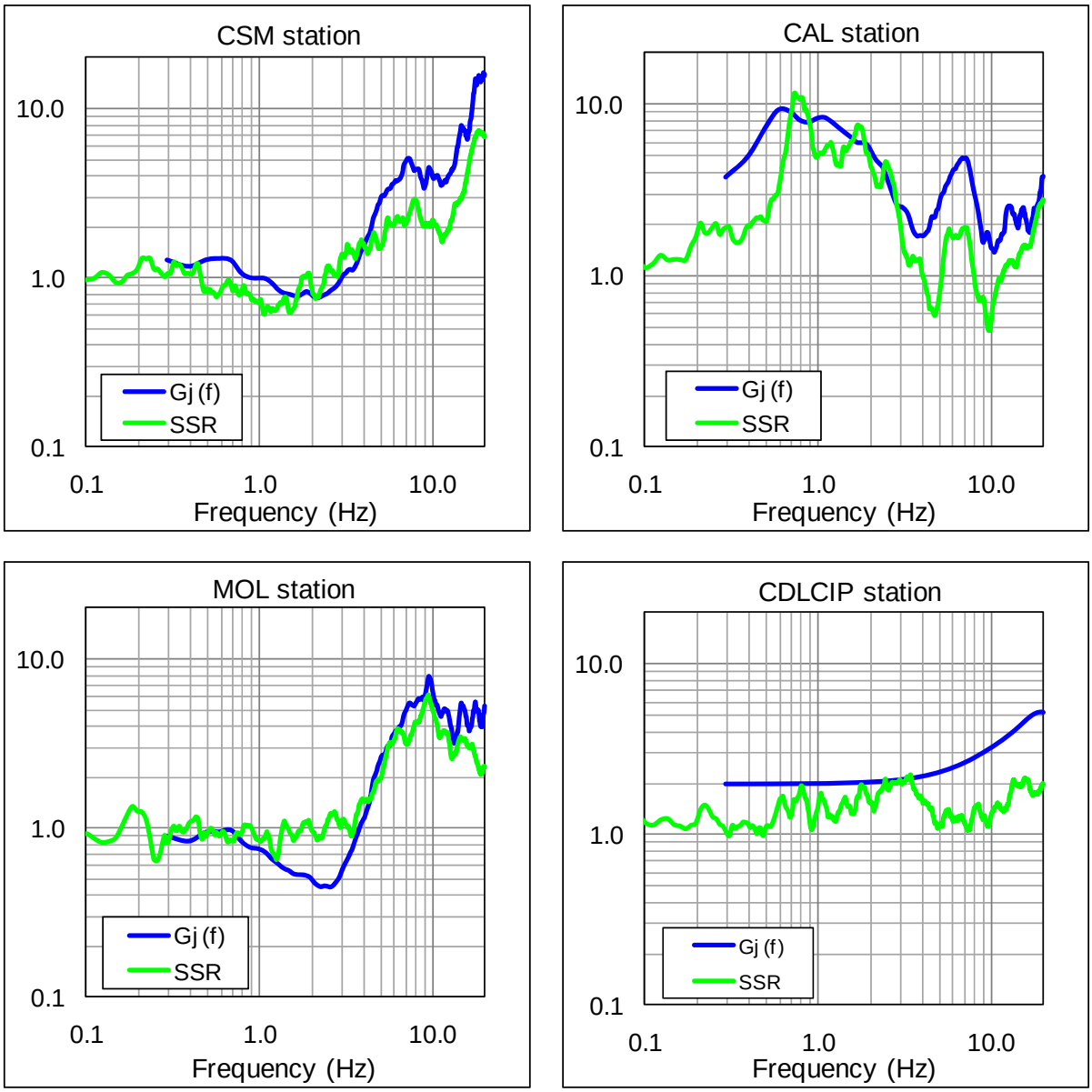

Figure 13. Comparison of site response with different techniques. The *Gj(f)* and the SSR are represented by the blue and green lines, respectively.

5.2 Surface Geology and Local Surface Conditions

As mentioned in subchapter 2.1, the locations of CSM, CAL, MOL and CDLCIP stations are on Quaternary alluvial deposits (Figure 5). Figure 14 shows the comparison of site amplification factors $G_j(f)$ for these four stations. It is noted that $G_j(f)$ for CSM, MOL and CDLCIP stations have larger amplifications at frequencies above 4 Hz, but nevertheless a considerable variation is observed in CAL station, located also in Quaternary deposits, in which the amplification values are much higher at frequencies below 4 Hz.

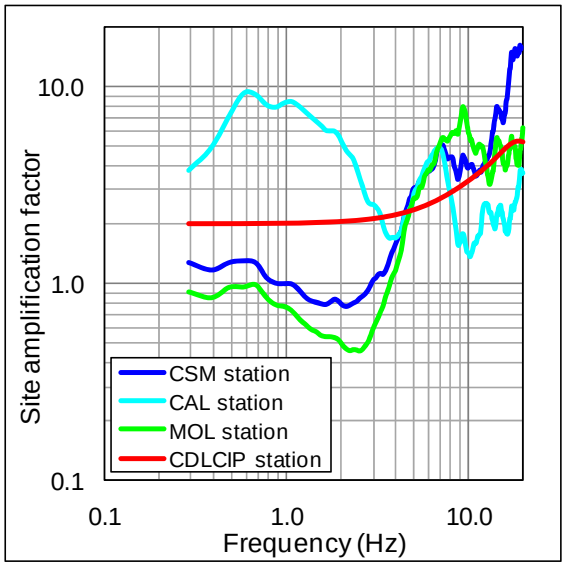

Figure 14. Comparison of $G_j(f)$ for CSM, CAL, MOL and CDLCIP stations.

To understand what was mentioned above, Figures 15 and 16 will help in understanding the differences between CAL station and other stations. Figure 15 shows the soil type map of Lima city developed by CISMID in 2003 with the support of the recognized Peruvian geologist Alberto Martinez Vargas, under the request of the APESEG (Peruvian Association of Insurance Companies) (Aguilar 2005); and Figure 16 displays the superposition of geological and soil type maps of Lima city.

According to Figure 16, CSM, CDLCIP and MOL stations are located on alluvial gravel overlying the denser Lima Conglomerate. Alluvial gravel covers a large portion of Lima city, and presents a good geomechanic behavior (Aguilar 2005). On the other hand, CAL station is located on soft soil, which is conformed by a 5 to 15 m thick layer of soft saturated clay and organic soil (Aguilar 2005).

The cases mentioned above prove once more that each soil type responds differently when subjected to ground motion from earthquakes, and as it has long been known, usually, that the younger, softer soils amplify ground motion bigger than older, more competent soils or bedrock (Steidl et al. 1996).

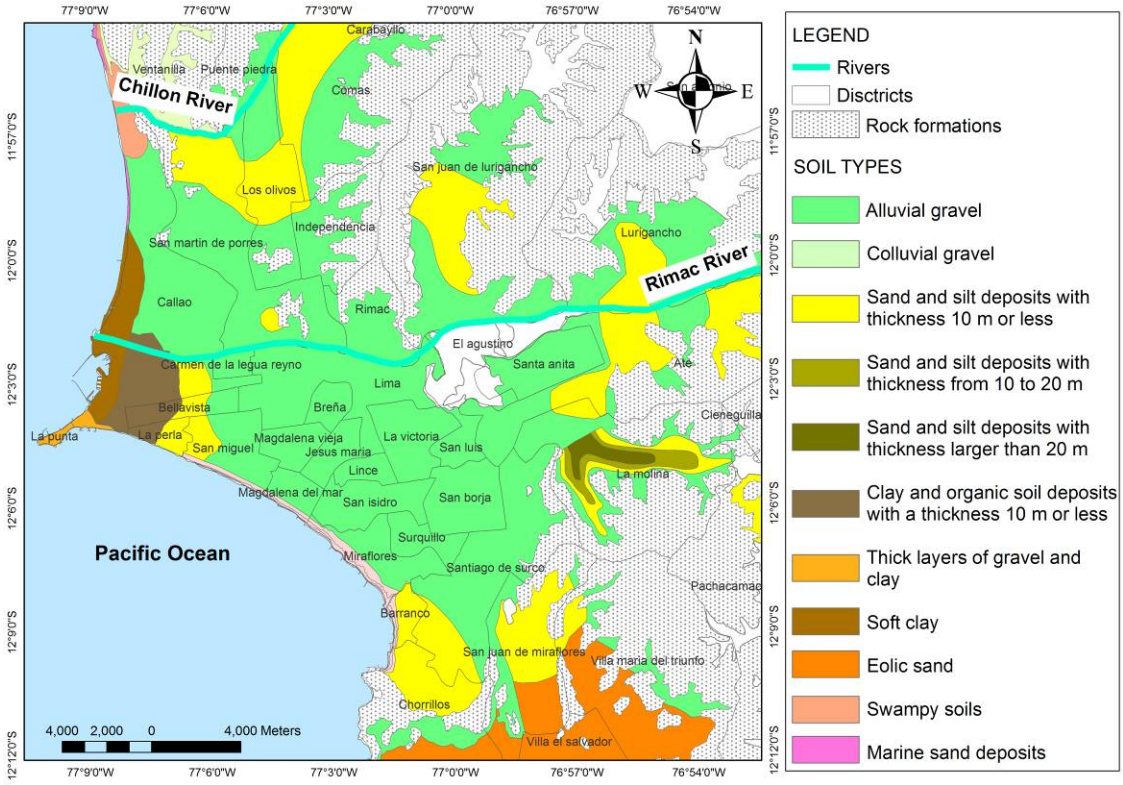

Figure 15. Soil type map of Lima city (CISMID 2003).

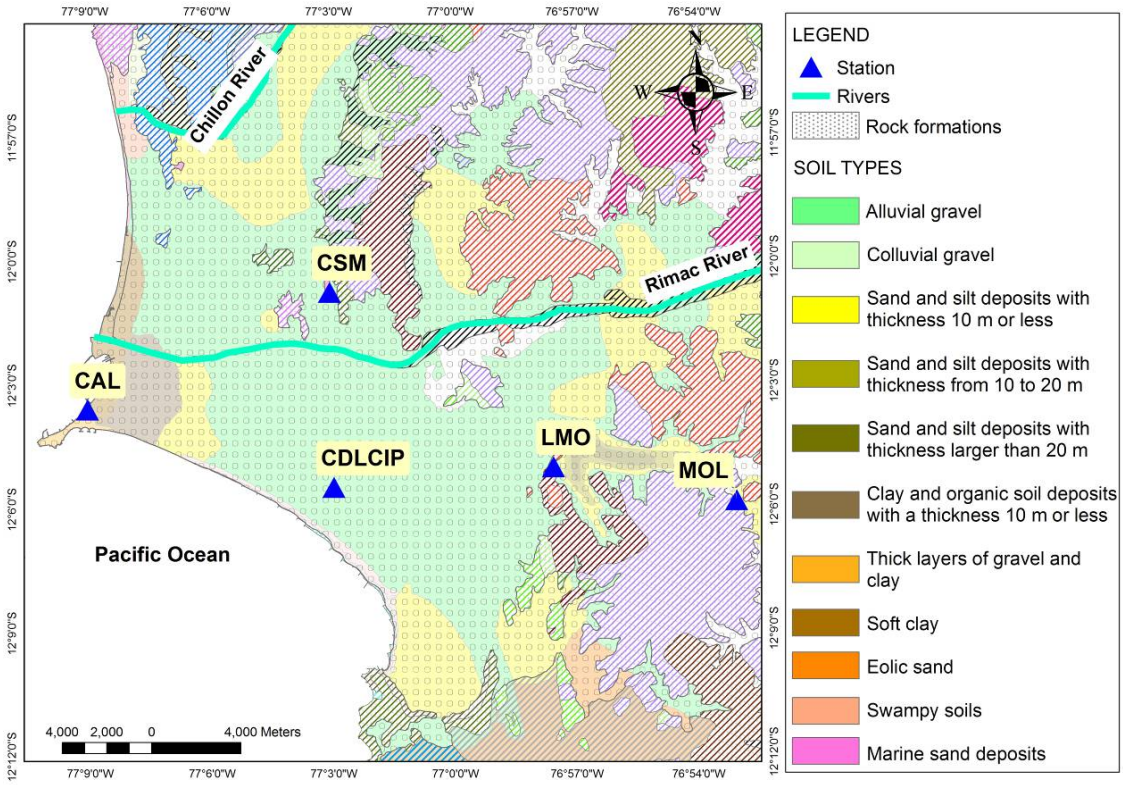

Figure 16. Superposition of geological and soil type maps of Lima city with stations.

5.3 Q_S–values

Figure 12 shows the Q_S–values as a function of frequency. In this figure, if it is examined in details, there is a conspicuous trough in the frequency range between 5 and 6 Hz. As known, higher frequency values provide close surface depth data whereas lower frequency values shed light on deep sections of the ground. So, if Figure 3 is observed, there is not enough data in the shallow part that can provide information in higher frequencies. That is the reason that for this study only is proposed one trendline because of previous studies as Takemura et al. (1991) demonstrated when the same area of study is reanalyzed with new additional data with more uniform distribution, Q_S-value as function of frequencies changes.

In Figure 4, a conspicuous peak in the same frequency range is also observed, and this occurs because the Qs-value along the wave propagation path influences the form of the source spectrum.

5.4 Analysis of Non-linearity of the Soil

On August 15, 2007, a strong offshore earthquake hit the coast of Central Peru. The epicenter was located at 150 km SSE of Lima city. This earthquake, also known as the Pisco earthquake, had a magnitude of 8.0 Mw and was at a focal depth of between 26 km and 39 km according to the United States Geological Survey (USGS 2008). The maximum peak ground acceleration recorded in Lima city was of 115.2 gal in La Molina district (Bernal and Tavera 2007). Figure 17 displays the acceleration time history recorded by CAL station. It is found that the rupture process of the main shock was composed of two major events, separated by 60 to 70 seconds (Bernal and Tavera 2007). In the present study, the influence of non-linearity on the site response is evaluated during the Pisco earthquake.

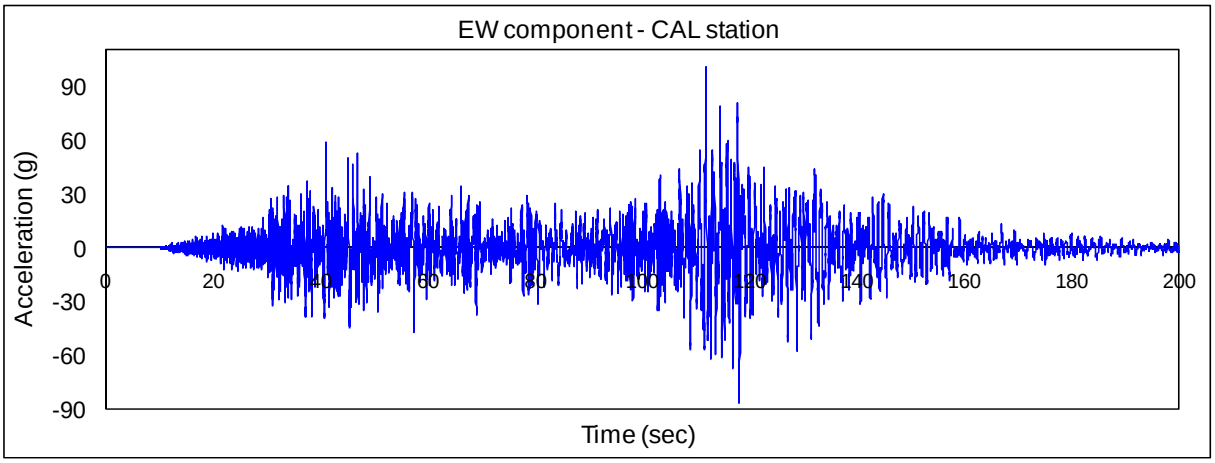

Figure 17. Acceleration time history recorded by CAL station during the Pisco earthquake.

From the spectral inversion method, Q_S-value and $G_j(f)$ at reference site are already known. To analyze the influence of the soil's non-linearity on the $G_j(f)$ at CSM, CAL, MOL and LMO stations, first the source amplitude spectrum $S_i(f)$ of the Pisco earthquake is calculated applying equation (1). After that, equation (4) is applied to get the site amplification factor during this strong ground motion where another amplification factor $G_{ij}(f)$ is newly defined for avoiding confusion

$$G_{ij}(f) = \frac{O_{ij}(f) R_{ij}}{S_i(f) \exp\left(-\pi R_{ij} f / Q_S(f) V_S\right)} \tag{4}$$

where, $O_{ij}(f)$ is the vectorial summation, $S_i(f)$, is the source spectrum and $Q_S(f)$ is the Q_S-value, this equation is taken of the study realized by Takemura et al. 1991. Due to the complex rupture process of the Pisco earthquake, the S-wave portion of the two horizontal components is analyzed for the main shock composed by the 1st and 2nd main events, and also for the first and the second main events. Figure 18 shows the site amplifications factor for the main shock, 1st and 2nd main rupture $G_{ij}(f)$ represented by the yellow, red and green lines, respectively with observed peak velocities of two horizontal components on the ground surface. In Figure 18 the amplification factor $G_j(f)$ obtained by the spectral inversion is also superposed, represented by the blue line. No systematic change is found for the difference between $G_j(f)$ obtained by the inversion analysis and $G_{ij}(f)$ for the main shock, 1st and 2nd main ruptures, namely there is not found explicit evidence of strong-motion deamplifications, accompanied by changes in resonant frequencies (Beresnev and Wen 1996). Thus, it is concluded that nonlinear response of the soils was not detected at acceleration levels below 115.2 gal during the Pisco earthquake.

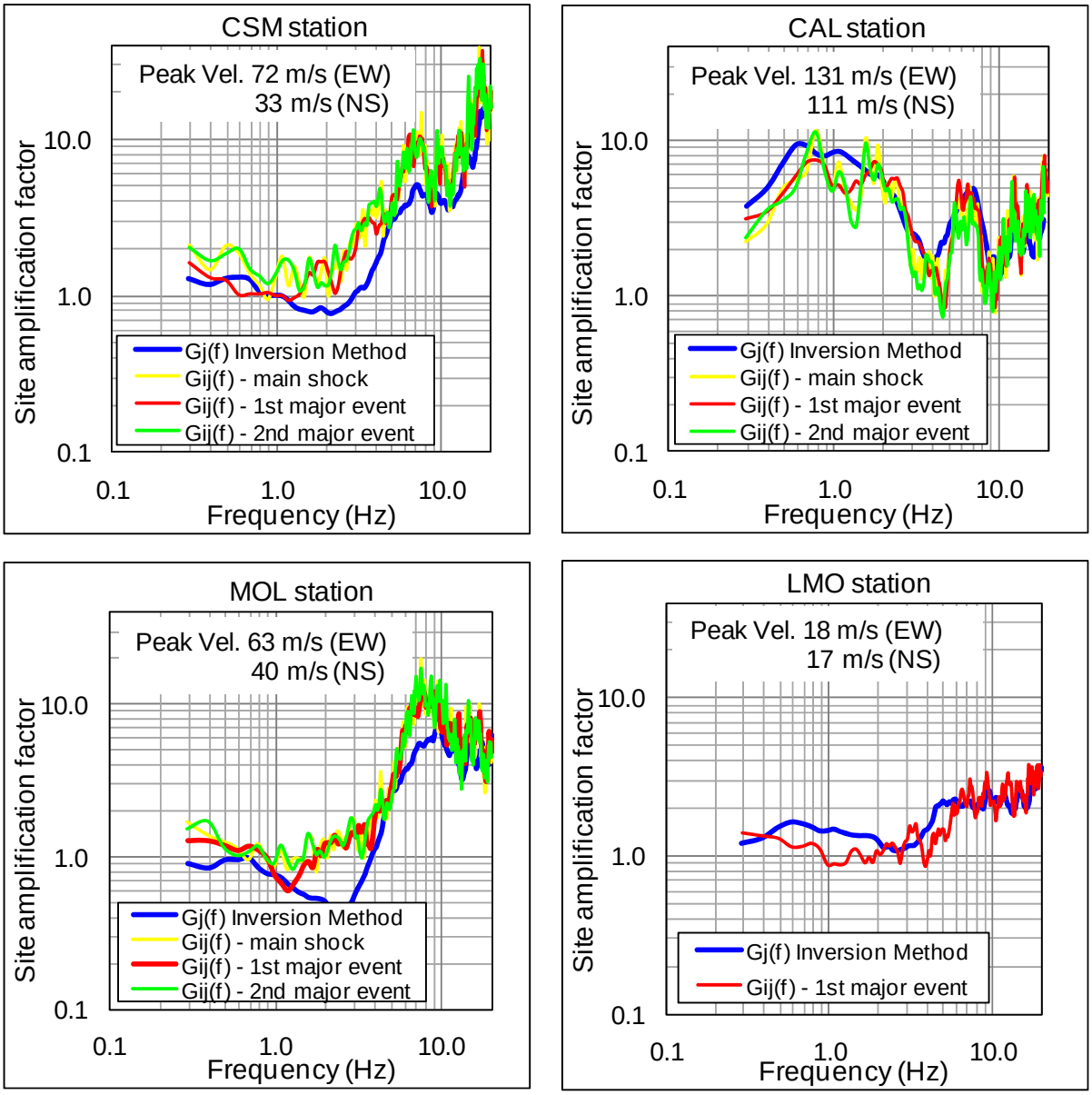

Figure 18. Analysis of non-linear site effect during the Pisco earthquake. The amplification factor $G_{ij}(f)$ for the main shock, 1st and 2nd rupture processes are indicated by the yellow, red and green lines, respectively. $G_j(f)$ obtained by the inversion analysis is also shown by the blue line.

5.5 Average S-wave Velocity and Site Amplification

In Figure 19 the site amplifications are compared with average S-wave velocity in top 30 meters of the S-wave profiles (Vs_{30}) for CSM, CAL and CDLCIP stations, and proposed linear relations between them at each frequency (0.5 Hz, 1.0 Hz, 2.0 Hz, 5.0 Hz, 10.0 Hz and 20.0 Hz). We know that Vs_{30} is only available for a few stations so far, but we want to show the possible relationships between Vs_{30} and SAF, and to improve our results for the future researches in the same area of interest.

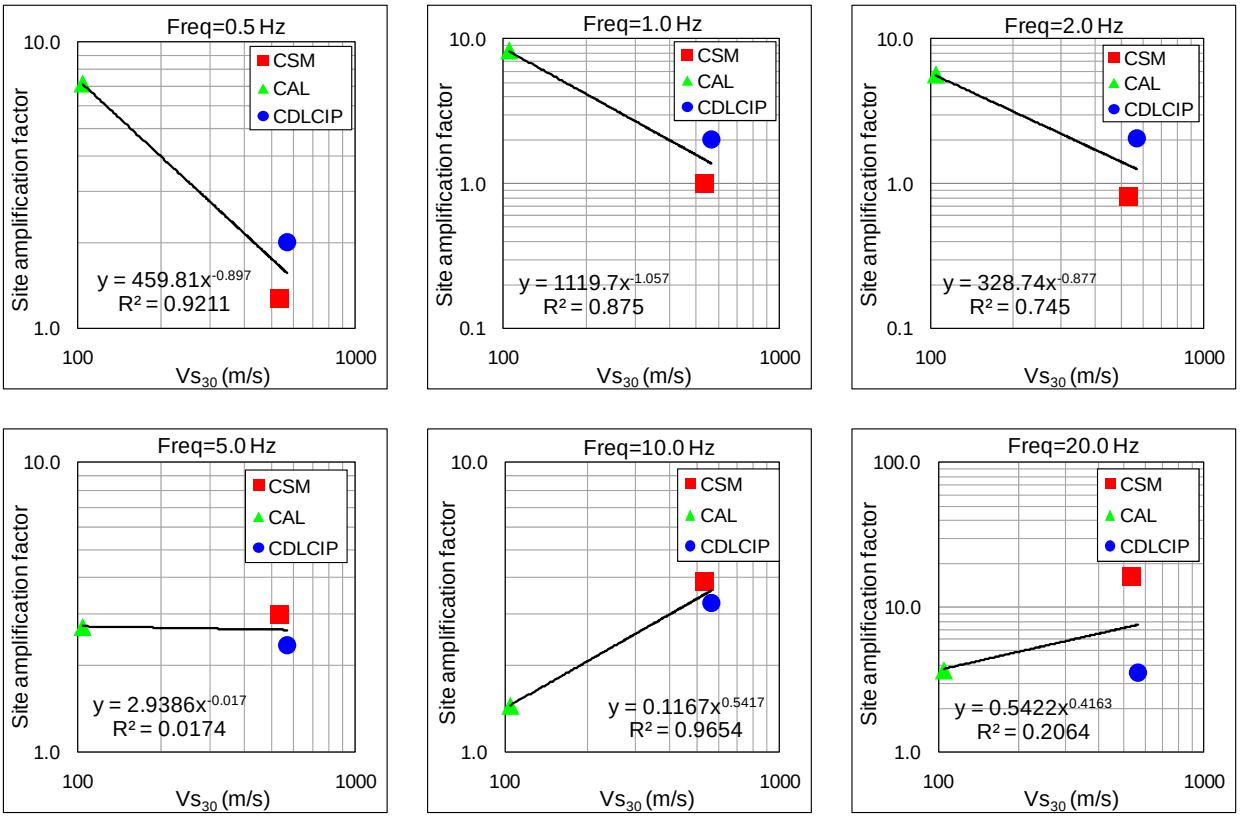

Figure 19. Relationship between site amplifications obtained from spectral inversion and Vs_{30} calculated for S-wave profiles at earthquake observation stations (CSM, CAL and CDLCIP stations) for different frequencies.

These relationships illustrate that Vs_{30} can be considered as a good indicator to estimate site amplification for frequencies less than 10.0 Hz; however for frequencies above 10.0 Hz is observed the trendline can not fit the calculated data well because the data are dispersive.

6. CONCLUSIONS

From the spectral inversion method, the site amplification factors for some areas of Lima city were evaluated from strong motion records observed along the Pacific coast of Lima city at 5 accelerometers. Out of the five stations used in this study, four stations (CSM, CAL, MOL and CDLCIP stations) are located on alluvial soil deposits belonging to the Quaternary Holocene. It is noted that $G_j(f)$ for CSM, MOL and CDLCIP stations have larger amplifications at frequencies above 4 Hz compared with CAL station, in which the amplification values are much higher at frequencies below 4 Hz. These differences between CAL station and other stations are due to the local subsurface conditions. CSM, CDLCIP and MOL stations are located on alluvial gravel overlying the denser Lima Conglomerate and CAL station is located on soft soil. As for MLO station, this station is located on

intrusive rock, so the $G_j(f)$ is less compared with the other stations.

The obtained results were confirmed with the results obtained by Cabrejos (2009) employing the Standard Spectral Ratio (SSR) in his study. There is a good agreement between both results, especially at frequencies below 5 Hz, although different techniques for estimating site response have been applied and different reference sites have been used.

About the Qs-value obtained in this study, there is a conspicuous trough in the frequency range between 5 and 6 Hz because there is not enough data in the shallow part that can provide information in higher frequencies. So it is recommendable that we should reanalyze these results with new data so that we should be able to get and improve our results.

The influence of non-linearity on the site response is evaluated during the Pisco earthquake, and it is concluded that nonlinear response of the soil was not detected at acceleration levels below 115.2 gal during this strong ground motion.

Relationship between site amplifications obtained from spectral inversion and Vs_{30} are proposed for frequencies 0.5 Hz, 1.0 Hz, 2.0 Hz, 5.0 Hz, 10.0 Hz and 20.0 Hz using the few data that it is currently available. So it is strongly recommendable to get information of another accelerometer stations located in Lima city to estimate better relationships for evaluating the local site effect.

7. ACTION PLAN

Currently a new international research program named “Science and Technology Research Partnership for Sustainable Development (SATREPS)” has just started and will continue for the five year period. The project aims to conduct a comprehensive research towards earthquake and tsunami disaster mitigation in Peru considering regional characteristics, under strong collaboration among researchers of Peru and Japan. So, I have the objective of applying the knowledge and experience that I gained here in this project, especially in strong motion prediction and development of seismic microzonation.

ACKNOWLEDGEMENT

I am really indebted to Prof. Dr. Hiroaki YAMANAKA -Tokyo Institute of Technology- who sincerely supervised and guided me during this work. I would like to send my appreciation to Dr. Toshiaki YOKOI and all the staff in Building Research Institute for their help and for their support. I would like to express my deepest gratitude to my colleagues in my institute –Earthquake Research Department- for their highly intensive efforts during this research. I thank Ms. Elsie Benedit Jaimin, Mr. Roberto Armando Torres Corredor and Mr. Hussam Eldein Zaineh Adel Wasfieh whose comments improved the paper, and Mr. Jonathan Cabrejos Hurtado for providing information personally collected. Also, I would like to express my recognitions to my colleagues in Yamanaka sensei Lab. for their help and their support during my study in Yamanaka sensei Lab. Finally, I truthfully appreciate the incessant encouragement offered by all of my family members for their support and their encouragement, and Mr. Akio Saito our course coordinator for taking care of me during my stay here in Japan.

This research was supported by Japan International Cooperation Agency (JICA) in cooperation with National Graduate Institute for Policy Studies (GRIPS) and International Institute of Seismology and Earthquake Engineering (IISEE).

APPENDIX-A: Available shear wave velocity profile for the stations used in this study

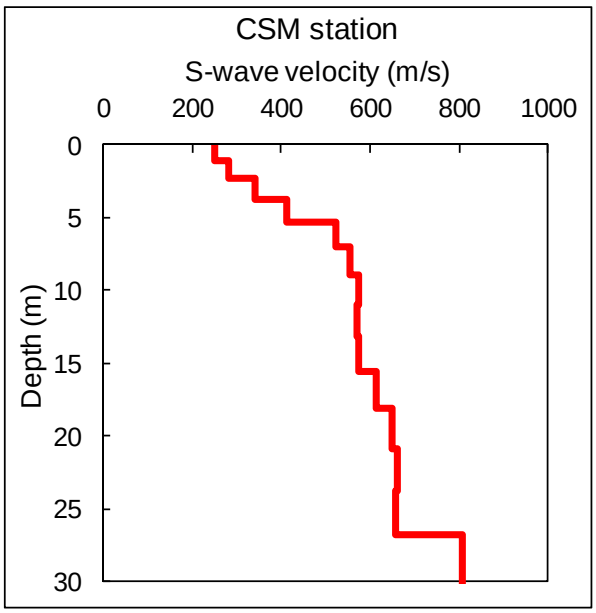

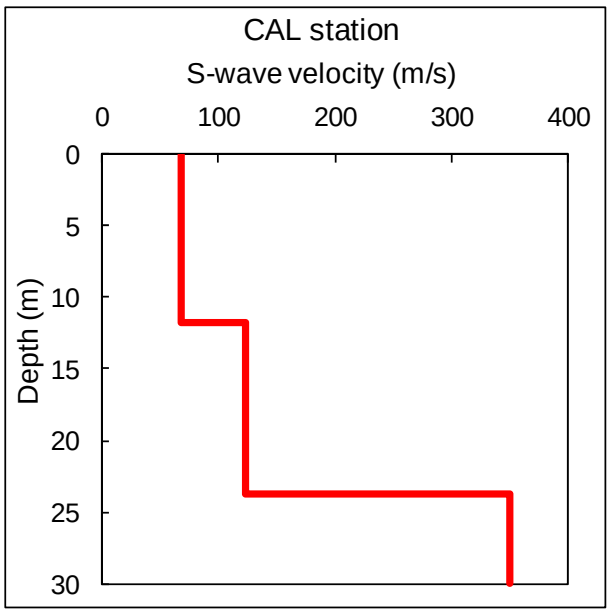

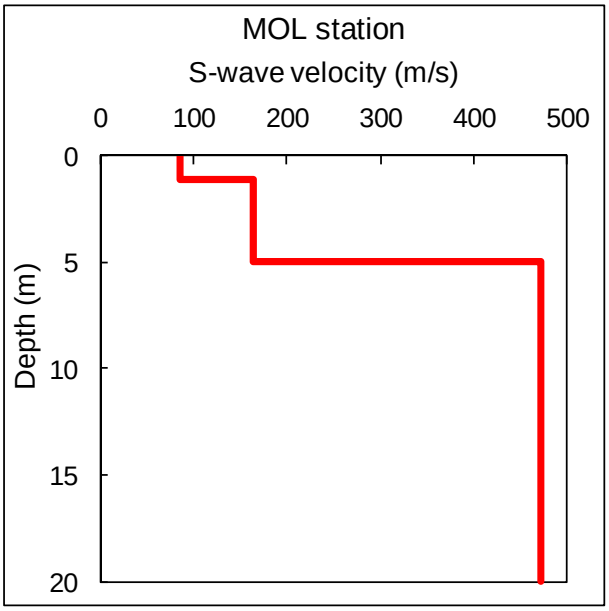

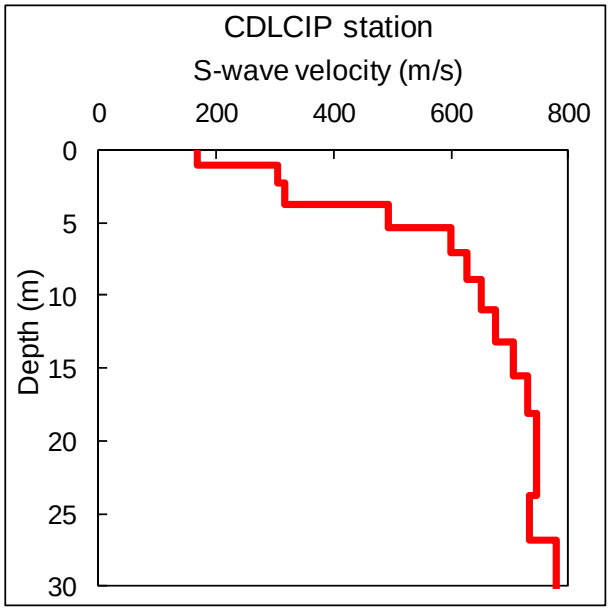

APPENDIX-B: Fourier acceleration amplitude spectral at all events

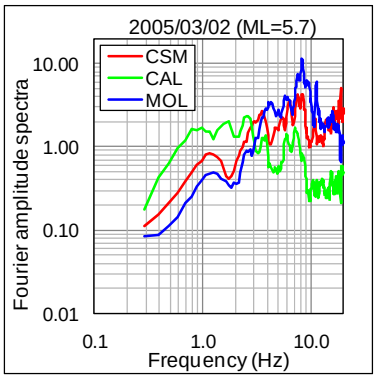

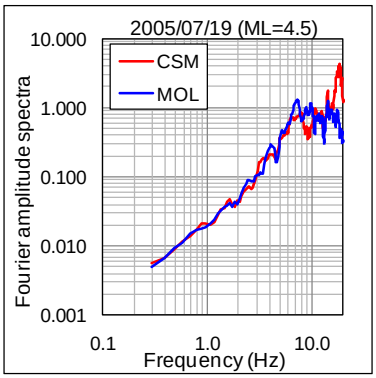

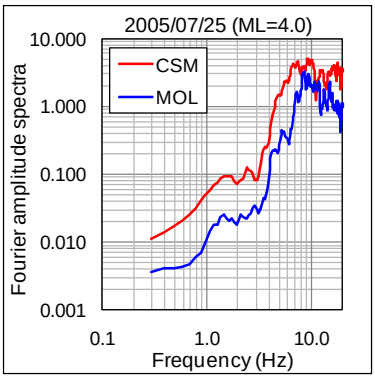

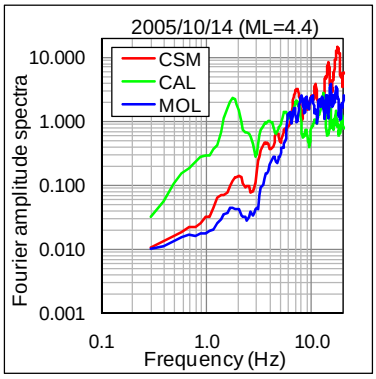

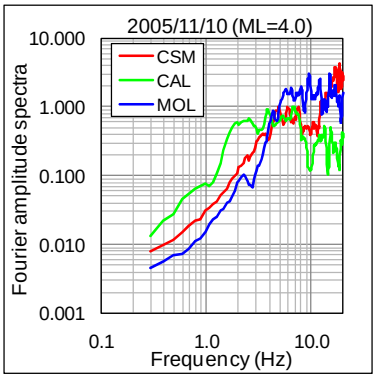

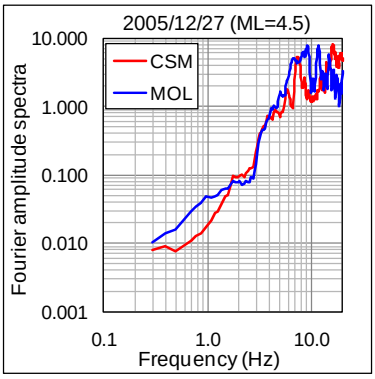

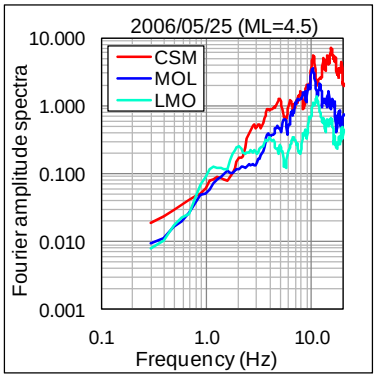

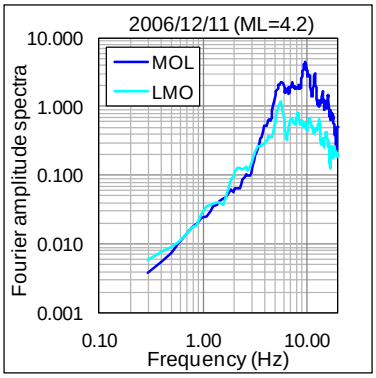

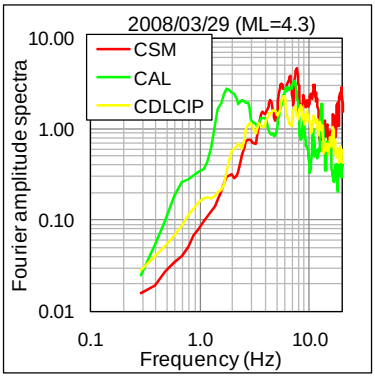

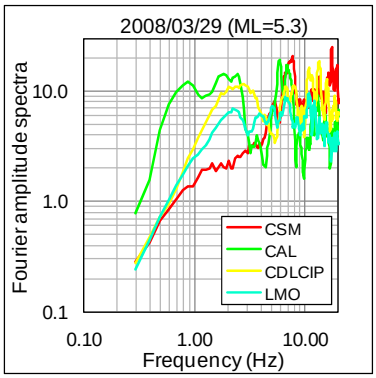

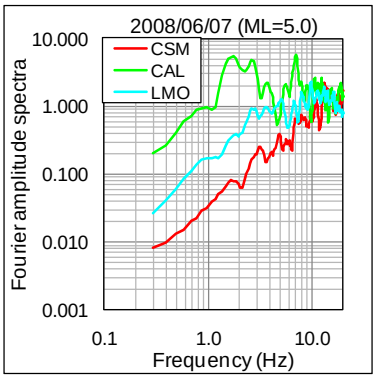

REFERENCES

Aguilar, Z., 2005, Seismic Microzonation of Lima City, Japan-Peru Workshop on Earthquake Disaster Mitigation, Japan Peru Center for Earthquake Engineering and Disaster Mitigation (CISMID), Faculty of Civil Engineering, National University of Engineering, Lima, Peru.

Andrews, D. J., 1982, Separation of Source and Propagation Spectra of Seven Mammoth Lakes aftershocks, Proceedings of Workshop 16, Dynamic Characteristics of Faulting, 1981, U.S. Geological Survey Open File Rep. 82-591, 437.

Beresnev, I. and Wen, K., 1996, Review: nonlinear soil response—a reality?, Bull. Seism. Soc. Am. 86, 1964–1978.

Bernal, I. and Tavera, H., 2007, Aceleraciones Máximas Registradas en la Ciudad de Lima: Sismo de Pisco del 15 de Agosto del 2007 (7.0 ML), Informe Preliminar (in Spanish).

Cabrejos, J., 2009, Amplificación Sísmica en la ciudad de Lima aplicando la Técnica de Cocientes Espectrales, Facultad de Ingeniería Civil, Universidad Nacional de Ingeniería (Lima, PE).

Espinoza, A. F., Husid, L. R., Algermissen, S. T. and De Las Casas, J., 1977, The Lima earthquake of October 3, 1974: Intensity Distribution, Bull. Seism. Soc. Am. 67(5), 1429-1439.

Haskell, N. A., 1960, Crustal Reflections of Plane SH waves, J. Geophys. Res., 65, 4147-4150

Husid, L. R., 1969, Características de terremotos – análisis general. Revista del IDIEM 8, 21-42, Santiago, Chile.

Husid, L. R., Espinoza A. F. and De Las Casas, J., 1977, The Lima earthquake of October 3, 1974: Damage Distribution, Bull. Seism. Soc. Am. 67(5), 1441-1472.

Iwata, T. and Irikura, K., 1986, Separation of Source, Propagation and Site Effects from Observed S-waves, Zisin II (J. Seismol. Soc. Jpn.), 39, 579-593 (in Japanese with English Abstract).

Iwata, T. and Irikura, K., 1988, Source Parameters of the 1983 Japan Sea Earthquake Sequence, J. Phys. Earth. 36, 155-184.

Le Roux, J.P., Tavares, C., and Alayza, F., 2002, Sedimentology of the Rimac-Chillon alluvial fan at Lima, Peru, as related to Plio-Pleistocene sea-level changes, glacial cycles and tectonics, Journal of South American Earth Sciences, 13, 499–510.

Lee, K. L. and Monge, J., 1968, Effect of soil conditions on damage in the Peru earthquake of October 17, 1966, Bull. Seism. Soc. Am. 58,937-962.

Lomnitz, C. and Cabré, R., 1968, The Peru earthquake of October 17, 1966, Bull. Seism. Soc. Am. 58, 645-661.

Martínez, A. and Porturas, F., 1975, Planos Geotécnicos para Lima, Perú. Análisis y Visión en Ingeniería Sísmica, Pontificia Universidad Católica del Perú, Lima, Perú (In Spanish).

Ozmen, O., 2009, Study on Site Effects using Strong Motion Data of BYT-NET array in Turkey, Individual studies by participant at the IISEE 40, 1-29.

Takemura, M., Ikeura, T., and Sato, R., 1990, Scaling Relations for Source Parameters and Magnitude of Earthquake in the Izu Peninsula Region, Tohoku Geophys. J. (Sci. Rep. Tohoku

Univ., Ser. 5), 32, 77-89.

Takemura, M., Kato, K., Ikeura, T., and Shima, E., 1991, Site Amplification of S-Waves from Strong Motion Records in Special Relation to Surface Geology, J. Phys. Earth, 39, 537-552.

Kanamori, H., 1972, Mechanism of Tsunami earthquakes, Phys. Earth Planet. Inter., 6, 346-359.

Kato, K., Takemura, M., Ikeura, T., Urao, K., and Uetake, T., 1992, Preliminary Analysis for Evaluation of Local Site Effect from strong Motion Spectra by an Inversion Method, J. Pyhs. Earth, 40, 175-191.

Phillips, W. S. and Aki, K., 1986, Site amplification of coda waves from local earthquake in central California, Bull. Seism. Soc. Am., 76, 627-648.

Repetto, P., Arango, I., and Seed, H. B., 1980, Influence of site characteristics on building damage during the October 3, 1974 Lima earthquake, Report-Earthquake Engineering Research Center, College of Engineering, University of California, Berkeley, California, NTIS, 80–41.

Steidl, J. H., Tumarkin, A. G., and Archuleta, R. J., 1996, What is a reference site?, Bull. Seism. Soc. Am., 86, 1733-1748.

Stephenson, W.R., Benites, R.A. and Davenport, P.N., 2009, Localized coherent response of the La Molina basin (Lima, Peru) to earthquakes, and future approaches suggested by Parkway basin (New Zealand) experience, Solid dynamics and earthquake engineering, 29(10), 1347-1357.

United States Geological Survey, 2008, Peru Earthquake Information. http://earthquake.usgs.gov/eqcenter/eqinthenews/2007/us2007gbcv/. Page accessed on March 1, 2008.